Asymmetric Binding of the High-Affinity $Q_H^{\bullet-}$ Ubisemiquinone in Quinol Oxidase (bo_3) from *Escherichia coli* Studied by Multifrequency Electron Paramagnetic Resonance Spectroscopy†

S. Grimaldi,‡ T. Ostermann,§,|| N. Weiden,⊥ T. Mogi,#,@ H. Miyoshi,▽ B. Ludwig,|| H. Michel,§ T. F. Prisner,‡ and F. MacMillan*,‡

Institut für Physikalische und Theoretische Chemie and Institut für Biochemie, J. W. Goethe Universität Frankfurt, D-60439 Frankfurt am Main, Germany, Max-Planck Institut für Biophysik, D-60528 Frankfurt am Main, Germany, Department of Biological Sciences, Graduate School of Science, University of Tokyo, Hongo, Bunkyo-ku, Tokyo 113-0033, Japan, ATP System Project, Exploratory Research for Advanced Technology (ERATO), Japan Science and Technology Corporation (JST), Nagatsuta, Midori-ku, Yokohama 226-0026, Japan, Division of Applied Life Sciences, Kyoto University, Kyoto 606-8502, Japan, and Institut für Physikalische Chemie, Technische Universität Darmstadt, D-64287 Darmstadt, Germany

Received January 6, 2003; Revised Manuscript Received March 7, 2003

ABSTRACT: Ubiquinone-2 (UQ-2) selectively labeled with ^{13}C ($I = {}^1/_2$) at either the position 1- or the 4-carbonyl carbon is incorporated into the ubiquinol oxidase bo_3 from *Escherichia coli* in which the native quinone (UQ-8) has been previously removed. The resulting stabilized anion radical in the high-affinity quinone-binding site ($Q_H^{\bullet-}$) is investigated using multifrequency (9, 34, and 94 GHz) electron paramagnetic resonance (EPR) spectroscopy. The corresponding spectra reveal dramatic differences in ^{13}C hyperfine couplings indicating a strongly asymmetric spin density distribution over the quinone headgroup. By comparison with previous results on labeled ubisemiquinones in proteins as well as in organic solvents, it is concluded that $Q_H^{\bullet-}$ is most probably bound to the protein via a one-sided hydrogen bond or a strongly asymmetric hydrogen-bonding network. This observation is discussed with regard to the function of Q_H in the enzyme and contrasted with the information available on other protein-bound semiquinone radicals.

Quinone molecules are involved in many of the oxidation−reduction processes of respiration and photosynthesis in living cells. Because of their long hydrophobic tail they are able to freely diffuse in membranes (e.g., quinone pools) or are able to bind to membrane proteins in well-structured binding pockets where they act as one- or two-electron gates and are thus able to couple electron transfer to proton translocation across the membrane (*1*). The fully oxidized quinone form is commonly found in these binding sites, although sometimes they can be observed in the one-electron reduced semiquinone form ($Q^{\bullet-}$), while the two-electron reduced quinol form usually diffuses away from the binding pocket. It has been shown that structurally identical quinones can have very different chemical properties when bound in different sites within a protein (*2*). This is probably because of specific interactions of the quinone molecule with its immediate protein environment, and which is believed to fine tune the electronic structure of the quinone for optimum function. These specific interactions are suggested to involve hydrogen bonds from the two carbonyl groups of the quinone to the protein, but may also involve π interactions with the aromatic ring and the hydrophobic isoprenyl side-chain.

The stable secondary electron acceptors, Q_A and Q_B,[1] of the purple bacterial photosynthetic reaction center (bRC) are the most well-studied and best-characterized quinone binding sites in membrane proteins (*2*, *3*). Q_A and Q_B are mainly ubiquinone derivatives in bacteria but may also be naphthoquinones and are plastoquinones in higher plants. Although Q_A and Q_B are of similar or even identical molecular structure, Q_A acts only as a one-electron acceptor, while Q_B

† This work was supported by the Deutsche Forschungsgemeinschaft (Sfb 472, P15) and the Hermann-Willkomm Stiftung (to F.M.).

* Corresponding author. Fax: (+49 69) 79829404. Telephone: (+49 69) 79829593. E-mail: macmillan@chemie.uni-frankfurt.de.

‡ Institut für Physikalische und Theoretische Chemie, J. W. Goethe Universität Frankfurt and Centre for Biological Magnetic Resonance.

§ Max-Planck Institut für Biophysik.

|| Institut für Biochemie, J. W. Goethe Universität Frankfurt.

⊥ Technische Universität Darmstadt.

Tokyo Institute of Technology.

▽ Kyoto University.

@ Japan Science and Technology Corporation.

[1] Abbreviations: A_1, secondary electron acceptor in type-I reaction centers; a_{iso}, isotropic hyperfine coupling; CIDEP, chemically induced dynamic electron polarisation; COX, cytochrome *c* oxidase; CP-MAS NMR, cross polarization magic angle spinning nuclear magnetic resonance; Cw, continuous wave; β-DM, *n*-dodecyl-β-D-maltoside; DME, 1,2-dimethoxyethane; DPPH, (α,α')-diphenyl-β-picrylhydrazyl; EPR, electron paramagnetic resonance spectroscopy; ENDOR, electron nuclear double resonance spectroscopy; ESEEM, electron spin−echo envelope modulation spectroscopy; FTIR, Fourier transform infrared spectroscopy; G, Gauss; hf, hyperfine; HYSCORE, hyperfine sublevel correlation spectroscopy; LDAO, *N*,*N*-dimethyldodecylamine *N*-oxide; mTHF, 2-methyltetrahydrofuran; PSI, photosystem I; PSII, photosystem II; Q_A, Q_B, primary and secondary stable electron acceptors in type II reaction centres; Q_H, Q_L, high- and low-affinity ubiquinone-binding sites of quinol oxidase; Q_0, Q_i, quinones of the cytochrome bc_1 complex; QOX, quinol oxidase; bRC, bacterial reaction centre; UQ-n, ubiquinone, *n* is the number of isoprenyl units.

10.1021/bi034010z CCC: $25.00
Published on Web 04/24/2003

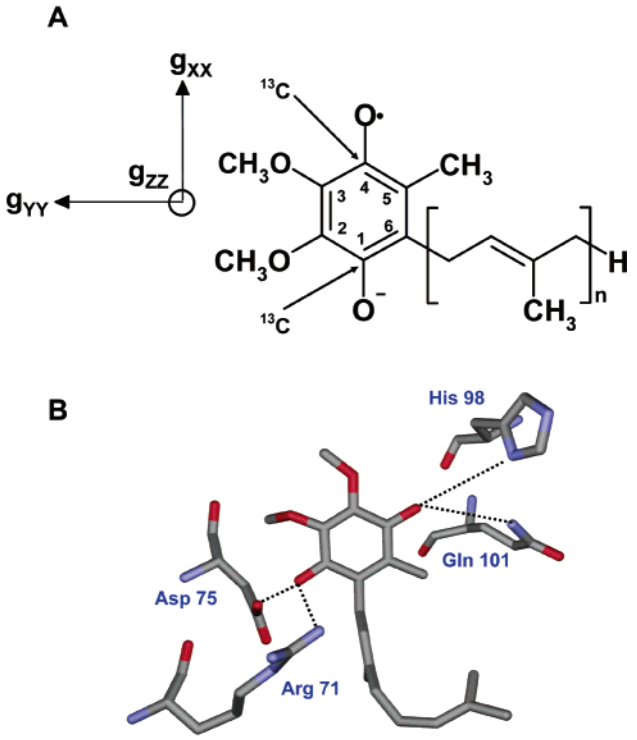

FIGURE 1: (A) Atomic numbering of UQ-n. The direction of the components of the **g** tensor with respect to the molecular axes is also indicated. (B) Modeled quinone in the structure of cytochrome bo_3 from *E. coli* as proposed by ref *10*.

accepts two electrons and two protons and diffuses out of its binding site (*2*).

A variety of spectroscopic techniques (e.g., FTIR (*4*), RAMAN (*5*), and CP-MAS NMR (*6*)) have been used to investigate the function and interaction of such quinones within their binding sites. Electron paramagnetic resonance (EPR) spectroscopy is also a very suitable tool for studying the radical anions of such molecules and has also been applied extensively to $Q_A^{\bullet-}$ (for a recent review, see ref *3*).

The respiratory chain is another rich source of quinones. Nearly all the membrane proteins in the respiratory chain are known to require quinones to catalytically function. The bo_3-type quinol oxidase (QOX) is a transmembrane protein involved in the aerobic respiratory chain of the Gram-negative bacterium *Escherichia coli* and is closely related to the mitochondrial cytochrome *c* oxidase (COX) in many aspects of its structure and function (for a recent review, see ref *7*). Indeed, it acts as a redox-driven proton pump that couples the vectorial translocation of protons across the membrane to the reduction of molecular oxygen to water. The major difference between both proteins, however, is the nature of the electron donating substrate: cytochrome *c* oxidases typically use the water-soluble protein cytochrome *c* as the electron donor, whereas quinol oxidase uses a membrane soluble ubiquinol molecule (in *E. coli* UQ-8, Figure 1A). QOX has been proposed to have up to two ubiquinone binding-sites, one with high (Q_H) and one with low (Q_L) affinity for ubiquinone (*8*, *9*), whereby electrons are transferred from the Q_L site to the next electron acceptor (heme *b*) via the Q_H site (*9*).

A crystal structure model of QOX was recently published at a resolution of 3.5 Å, which indicated that the overall structure of this complex is quite similar to that of cytochrome *c* oxidase (*10*). The crystals used for this structural model, however, did not contain bound quinones; thus, their exact location is still unresolved. A functional study of site-directed mutants was used to propose a model for the possible Q_H binding site, which is located in subunit I close to heme *b* (*10*). In this model, Q_H is predicted to form up to four hydrogen bonds with the protein: Asp75 and Arg71 to the 1-carbonyl oxygen and His98 and Gln101 to the 4-carbonyl oxygen (see Figure 1B).

EPR spectroscopy is a valuable tool for investigating semiquinone binding in proteins as has been demonstrated previously (e.g., ref *3*). X-band cw EPR has demonstrated that the Q_H site stabilizes a semiquinone radical anion (*11*, *12*). Direct evidence of a specific interaction of $Q_H^{\bullet-}$ with the immediate protein environment has been obtained using pulsed EPR spectroscopy (*13*). The pulsed EPR technique, electron spin−echo envelope modulation spectroscopy (ESEEM) revealed a strong, specific interaction of the unpaired electron of $Q_H^{\bullet-}$ with a peptide nitrogen nucleus that is consistent with the presence of a hydrogen bond between $Q_H^{\bullet-}$ and this nitrogen. Furthermore, based on the magnitude of the proton hyperfine coupling assigned to the methyl group at position 5 (Figure 1A) (*14*), it was suggested that this hydrogen bond is formed to the 1-carbonyl oxygen (*13*, *14*). Cw electron nuclear double resonance spectroscopy (ENDOR) has demonstrated the presence of such exchangeable protons consistent with hydrogen bonding to the quinone oxygens (*14*, *15*).

One way in which such specific interactions can be studied in greater detail requires the use of exchanged quinones—either isotopically labeled quinones or chemically different quinones. ^{13}C-selectively labeled ubiquinones have been successfully used to study the binding of Q_A and Q_B in their different redox states as well as the distribution of the spin density on both anion radicals and has greatly extended the functional and structural information inferred from X-ray crystallographic studies of the oxidized ground state (for a review, see ref *16*).

Using this approach, both FTIR measurements (*17*−*19*) and Q-band (34 GHz) cw EPR measurements (*20*, *21*) concluded that the 4-carbonyl oxygen of Q_A (see Figure 1A) is strongly hydrogen bonded to the protein. The analysis of the observed ^{13}C-hyperfine tensor elements for quinones selectively labeled at positions 1 and 4 indicated asymmetric hydrogen bonding (*20*, *21*), while similar measurements performed on Q_B (*21*) revealed less asymmetry, also in accordance with FTIR measurements (*22*, *23*). These observed results were suggested to correlate the functional difference of both quinones. Comparable measurements of the same quinones in vitro revealed virtually symmetric hydrogen bonding as is expected in alcoholic solution (*24*).

It is well-established that the hyperfine (**hf**) tensor of the ^{13}C nucleus is very sensitive to its local environment and thus to the local molecular structure (e.g., bond angles and bond length (*25*−*27*)). As has been demonstrated for Q_A and Q_B, EPR spectroscopy of ^{13}C-labeled semiquinones recorded at typical EPR frequencies (around 9 GHz) are difficult to interpret because of the comparable magnitude of the g-anisotropy of the radical and ^1H- and ^{13}C-hyperfine tensors resulting in an unresolved spectrum (e.g., Figure 2D). To address the question of Q_H binding in QOX, we have developed a procedure for incorporating exogenous ^{13}C-

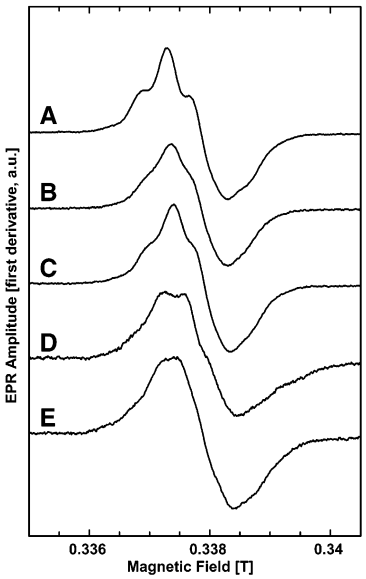

FIGURE 2: X-band EPR spectra of the bo_3−QOX of *E. coli* under reducing conditions. From top to the bottom: (A) native UQ-8, (B) after reconstitution with decylubiquinone, (C−E) after reconstitution with ^{12}C-UQ-2, $^{13}C_1$-UQ-2, and $^{13}C_4$-UQ-2, respectively. Experimental conditions: MW power = 0.1 mW; field modulation frequency = 100 kHz; field modulation amplitude = 1 G; temperature = 120 K; and microwave frequency = 9.45 GHz.

labeled quinones into the Q_H binding site. And to overcome the problem of spectral resolution, we apply multifrequency EPR to distinguish these different spectral contributions.

In this paper, the semiquinone radical anion that is selectively ^{13}C-enriched at either the 1- or 4- carbonyl position and reconstituted into the Q_H binding site of the bo_3 quinol oxidase is investigated using EPR spectroscopy at 9, 34, and 94 GHz. At 94 GHz, the magnetic field range spanned by the **g** tensor is sufficiently large that at the high-field edge practically only centers are observed whose **g** tensor *z* axis is oriented along the external magnetic field, allowing the direct measurement of the **hf** splitting along this direction (A_{ZZ}). Determination of ^{13}C hyperfine couplings and resulting assignment to a strongly asymmetrical binding of $Q_H^{\bullet-}$ in QOX is discussed.

MATERIALS AND METHODS

Sample Preparation. Ubiquinone-2 selectively labeled with ^{13}C ($I = {}^1/_2$) at the 1- or the 4-position of the quinone ring (i.e., [$^{13}C_1$]-UQ_2 or [$^{13}C_4$]-UQ_2) was synthesized as described previously in ref *28*.

The *E. coli* strain GO105/pJRHisA (*29*) was grown and isolated as described in ref *13*. Wild-type bo_3 enzyme with bound UQ-8 was purified as described previously (*30*). Native UQ-8 was removed by purification of QOX using *N*,*N*-dimethyldodecylamine *N*-oxide (LDAO) as the detergent, followed by detergent exchange with *n*-dodecyl-β-D-maltoside (β-DM). Reconstitution with exogenous decylubiquinone and UQ-2 analogues was performed directly in the EPR sample tube containing the protein, using quinone solutions dissolved in a very small amount of 2-propanol (1 μL). All samples were reduced with an excess of sodium ascorbate under a strict argon atmosphere.

Instrumentation. X-band EPR spectra were recorded using a Bruker ESP 300 spectrometer with a standard rectangular Bruker EPR cavity (ER4102T), and Q-band EPR spectra were recorded using a Bruker E-500 spectrometer with a standard Bruker resonator (ER 5106QT-W1). Both instruments were equipped with Oxford helium cryostats (ESR900 and CF935, respectively). W-band EPR spectra were acquired on a Bruker E680 spectrometer equipped with an Oxford helium-flow cryostat (CF935), a cylindrical Bruker Teraflex TE_{110} cavity, and a 6T Magnex superconducting magnet.

X-Band pulsed EPR measurements were performed on a Bruker eleXsys E-580 spectrometer using a standard dielectric resonator (MD5EN W1) equipped with an Oxford helium (CF 935) cryostat. 3 pulse ESEEM and Davies ENDOR experiments were performed as described previously (*13*, *31*) except that the microwave pulses (8 ns) were amplified using a 1 kW microwave amplifier (applied systems engineering).

EPR Data Analysis. In frozen solutions, anisotropic **g** and **hf** interactions are not averaged out, unlike in liquid solutions, and all molecular orientations relative to the magnetic field have to be considered. The spin Hamiltonian describing the magnetic interaction between the electron spin of the semiquinone radical and the nuclear spins $I = {}^1/_2$ (e.g., ^{13}C or ^1H nuclei) in an external magnetic field B_0 is given by

$$H_s = \mu_B \vec{B}_0 \tilde{\mathbf{g}} \vec{S} - \mathbf{g}_{nI} \mu_I \vec{B}_0 \vec{I}_I + \sum_J \vec{S} \tilde{\mathbf{A}}_I \vec{I}_I$$

where $\tilde{\mathbf{g}}$ is the electronic **g** tensor; $\tilde{\mathbf{A}}_I$ is the **hf** tensor of nucleus I with principal values $\{\mathbf{A}_{ii}\}$ ($i = x,y,z$); J is the number of coupled $I = {}^1/_2$ nuclei; and S, I_I, μ_B, and μ_I are the electron and nuclear spin operators and magnetons, respectively. Signals from molecules with all possible orientations relative to B_0 contribute to the EPR spectrum, which is therefore significantly broadened because of the **g** and **hf** tensor anisotropies. Spectra were simulated using a home-written simulation and fit program (*32*), written in Matlab. The measured **g** values were corrected for an offset against a known **g** standard (DPPH ($\mathbf{g} = 2.00351 \pm 0.00002$) and N @ C_{70} ($\mathbf{g} = 2.0021 \pm 0.0001$) for 94 GHz measurements).

RESULTS

Figure 2 shows the cw X-band EPR spectra of the bo_3 quinol oxidase from *E. coli* under reducing conditions at 120 K. The native ubisemiquinone radical $Q_H^{\bullet-}$ under nonsaturating conditions has a line width of ~1.0 mT (Figure 2A). In samples prepared in the presence of LDAO, no EPR signal from $Q_H^{\bullet-}$ is observed. Samples reconstituted with exogenous quinones reveal an EPR signal very similar to that of $Q_H^{\bullet-}$ (Figure 2B,C). ESEEM and ENDOR investigations of these reconstituted samples indicate that the reconstituted quinone is bound in the Q_H binding site (Figure 3, see Discussion).

Unlike the **g** value, which remains the same, the line width of the radicals reconstituted with selectively ^{13}C-labeled UQ-2 is strongly affected because of the additional ^{13}C−**hf** interaction. The observed line width at X-band increases to 1.42 mT and 1.18 mT for [$^{13}C_1$]-UQ-2 and [$^{13}C_4$]-UQ-2, respectively (Figure 2D,E).

At higher microwave frequencies, the **g** tensor of $Q_H^{\bullet-}$ can be better resolved (Figure 4). At Q-band (34 GHz), it has been shown that the **g** tensor anisotropy of $Q_H^{\bullet-}$ is only partially resolved (*13*, *14*) (Figure 4B). At 94 GHz, the resolution of the G_{ZZ} component is clearly observed, while

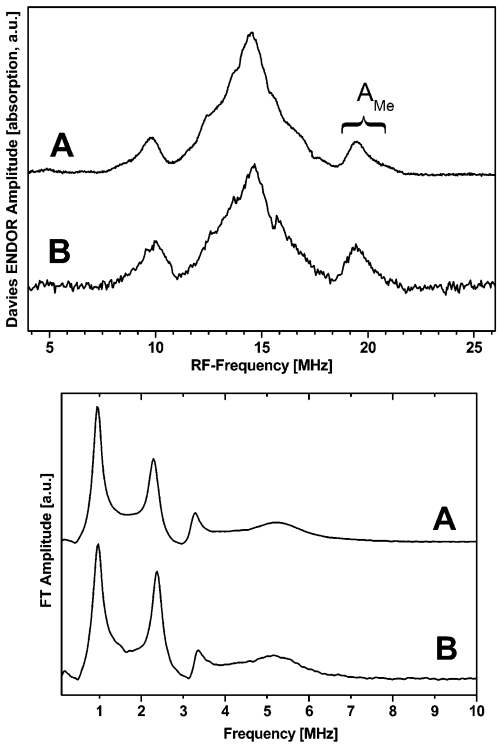

FIGURE 3: Davies ^{1}H-ENDOR (top) and Fourier transformed 3 pulse ESEEM (bottom) spectra of the bo_3−QOX of *E. coli* under reducing conditions. (A) Native UQ-8 and (B) after reconstitution with ^{12}C-UQ-2. Experimental conditions: Davies ^{1}H-ENDOR; microwave π-pulse length = 200 ns; radio frequency π-pulse length = 9 μs; and temperature = 20 K. Frequency domain 3-pulse ESEEM spectra: microwave $\pi/2$-pulse length = 8 ns; tau = 200 ns; and temperature = 20 K.

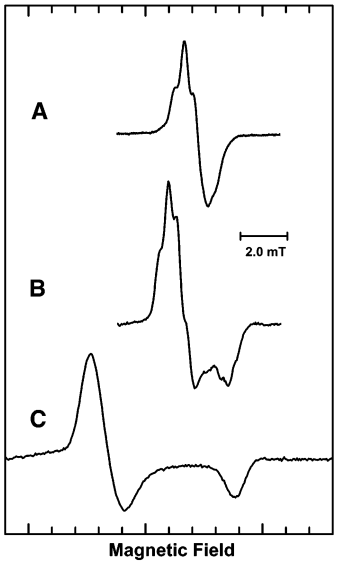

FIGURE 4: Cw-EPR spectra of $Q_H^{\bullet-}$ taken at (A) X-band (9.47 GHz), (B) Q-band (34.0 GHz), and (C) W-band (94.0 GHz) using a field modulation amplitude of 0.5G at T = 80 K. For all other experimental conditions, see Figures 2, 4, and 5.

the overall line shape remains predominantly axial (Figure 4C). A numerical simulation/fit of this spectrum indicates a slightly rhombic **g** tensor whose principal values (error ± 0.00005) are

$$G_{XX} = 2.00593,\ G_{YY} = 2.00543,\ G_{ZZ} = 2.00220,\ \mathbf{g}_{iso} = 2.00452$$

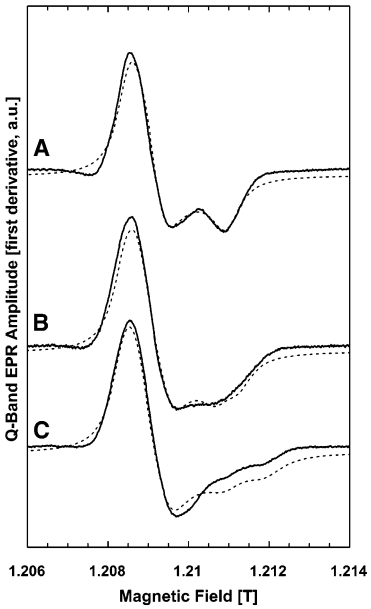

FIGURE 5: Q-band (34 GHz) EPR spectra of bo_3−QOX under reducing conditions. From top to the bottom: (A) reconstituted with unlabeled UQ-2 (^{12}C), (B) reconstituted with UQ-2 ^{13}C-labeled at the 1-carbonyl position, and (C) reconstituted with UQ-2 ^{13}C-labeled at the 4-carbonyl position. Experimental conditions: MW power = 1.2×10^{-3} mW; field modulation frequency = 100 kHz, field modulation amplitude = 3 G; T = 80 K; and microwave frequency = 33.98 GHz. Spectral simulations are performed using the **g** tensor given in the text, Table 1, ref *13*, and a line width of 3.5 G.

The increase in resolution of the $\tilde{\mathbf{g}}$ tensor at 94 GHz leading to a separation of the G_{ZZ} component is of great advantage when studying the ^{13}C-labeled compounds. The effect of ^{13}C labeling at the 1- and 4-carbonyl position is clearly observed at Q-band (Figure 5), but the magnitude of this ^{13}C−**hf** interaction (A_{ZZ}) along G_{ZZ} can be clearly determined from spectra taken at 94 GHz (Figure 6).

Simulation of these spectra allows a direct determination of the A_{ZZ} component of the $^{13}C_1$ and $^{13}C_4$ hyperfine tensor (Figure 5), which is assumed to be parallel to the G_{ZZ} component (see Discussion). These simulations have been carried out including explicitly hyperfine interactions from the methyl protons at position 5 (CH_3: ^{1}H−A_{XX} = 7.85 MHz, ^{1}H−A_{YY} = 12.80 MHz, and ^{1}H−A_{ZZ} = 8.4 MHz, ref *13*). Other smaller couplings (hydrogen bonded-, CH_2-, and methoxy-protons) are taken into account through use of an anisotropic line width parameter characterized by a Gaussian line shape. Observed components of ^{13}C hyperfine tensors used for simulations are given in Table 1.

Even at W-band, EPR spectra (solid lines) and simulations (dashed lines) can only provide an upper limit for the ^{13}C−A_{XX} and ^{13}C−A_{YY} components (Table 1) as these couplings only give rise to a broadening of the low-field feature in the spectrum. On the other hand, the A_{ZZ} components of the hyperfine coupling tensors are now well-resolved.

DISCUSSION

The primary aim of this paper is to analyze the electronic structure of $Q_H^{\bullet-}$ in the bo_3 quinol oxidase from *E. coli* as a consequence of the surrounding protein using a combination of selective ^{13}C isotope labeling and multi-frequency EPR spectroscopy. It has been previously demonstrated that the length of the isoprenoid side chain beyond the first

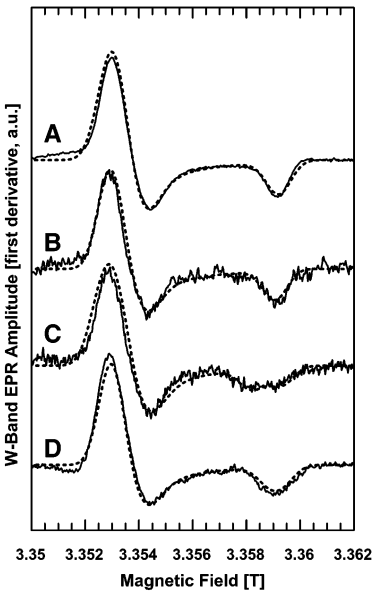

FIGURE 6: W-band (95 GHz) EPR spectra of bo_3−QOX under reducing conditions. From top to the bottom: (A) native UQ-8; (B) reconstituted with UQ-2; (C) ^{13}C-enriched at the 1-carbonyl position, and (D) ^{13}C-enriched at the 4-carbonyl position. Experimental conditions: MW power = 5×10^{-5} mW; field modulation frequency = 100 kHz; field modulation amplitude = 2 G, frequency = 100 kHz; T = 90 K; and microwave frequency = 93.95 GHz. Spectral simulations performed using the **g** and **hf** tensors given in the text, Table 1, ref *13*, and a line width of 4.5 G.

isoprenyl unit does not influence the spin density of such semiquinones and the intramolecular hyperfine couplings appreciably (*21*, *33*, *34*); thus, UQ-2 was used as an exogenous ubiquinone for the reconstitution experiments. Indeed, UQ-2 is the molecule used in all activity tests for QOX (*9*).

Although the multi-frequency EPR spectra shown here are a direct indication that a semiquinone is formed, it is very important to check that the species observed is similarly bound in the same binding pocket as that of the native quinone. For this purpose, several of the experimentally observed parameters were compared: (i) the **g** tensor, which is very sensitive to the electrostatic environment around the semiquinone, is identical within experimental error for the native and the ^{12}C-UQ-2$^{\bullet-}$ revealing a very small anisotropy (G_{XX} = 2.00593) as compared to other protein-bound ubiquinone radicals. Such G_{XX} values have been shown to indicate strong hydrogen bonding (*24*, *33*, *35*). Indeed, this value is lower than any other known protein-bound ubiquinone anion radical studied so far; (ii) ^{14}N-ESEEM spectroscopy clearly shows the characteristic quadrupolar interaction, which is the same for all samples used in this study and which is assigned to a peptide nitrogen nucleus as observed in the study of Grimaldi et al. (*13*) on the native $Q_H^{\bullet-}$ ubiquinone radical (Figure 3, bottom); and (iii) pulsed ^{1}H Davies ENDOR spectra of all these samples were very similar to that obtained from the native $Q_H^{\bullet-}$(Figure 3, top).

In particular, the strong proton coupling from the methyl group at position 5 (indicated in Figure 3, top), which ideally serves as sensitive monitor of the spin density, is not significantly altered with respect to values previously published (*13*−*15*). If the reconstituted UQ-2 and the native UQ-8 would be bound in a different fashion (e.g., symmetrically hydrogen-bonded), a dramatic alteration of such hyperfine couplings would be expected as has been shown previously using DFT calculations (*36*, *37*). Using CIDEP spectroscopy, the limiting case of a monoprotonated semiquinone has been studied, where such couplings can increase by a factor of 2 (*38*).

Taken together, these results indicate that the quinone signals arise from a specific quinone tightly bound within the Q_H binding pocket of bo_3 ubiquinol oxidase and not from quinones in detergent micelles and that the reconstitution method inserts UQ-2 into the native binding site. In particular, the electronic structure of the observed radical species is not dramatically altered upon reconstitution with UQ-2.

The increase of the line width with respect to the wild type, which is already clearly observable at the X-band, is due to the strong hyperfine coupling of the ^{13}C nucleus. These marked differences in this line width alteration indicate that both labels do not contribute to the EPR spectrum in an identical fashion. EPR measurements at higher frequencies are used to resolve the **g** tensor anisotropy, which then simplifies the analysis of the ^{13}C−**hf** interactions. From symmetry considerations, the ^{13}C **hf** tensors studied here are assumed to be collinear with the **g** tensor axes; thus, their z direction coincides with the normal of the plane of the molecule (Figure 1A), leading to the strongest **hf** coupling in the z direction. This is confirmed by DFT calculations (data not shown). Calculations of the magnitude and orientation of the **g** tensor have shown that these axes coincide with the molecular axes within a few degrees even in the case of asymmetric hydrogen bonding to the carbonyl groups (*39*)**.** The x direction of the **g** tensor is aligned with the axis connecting the carbonyl oxygens.

Because the spectra of reconstituted $^{13}C_1$-UQ-2 and $^{13}C_4$-UQ-2 in the Q_H site are clearly different, it must be concluded that the electron spin is asymmetrically distributed over the respective C-atoms of the quinone in the protein-binding site. Moreover, these spectra clearly show that $^{13}C_1$-UQ-2 exhibits a much larger ^{13}C splitting of the A_{ZZ} component than $^{13}C_4$-UQ-2. The quantitative analysis of this observation has been obtained through the simulations of the Q- and W-band spectra (see Table 1). The simulations allow the determination of the magnitude of the A_{ZZ} components of the $^{13}C_1$ and $^{13}C_4$ **hf** tensors and to give an estimation of the upper limit of the two other components A_{XX} and A_{YY}. The hyperfine tensor is to a good approximation axially symmetric about the p_z orbital (that is about the z direction) as expected for a carbon atom in a π radical in which the anisotropy in the coupling is caused by spin density of a p orbital essentially fixed in space and $|A_{zz}|$ is larger than $|A_{xx}|$ and $|A_{yy}|$. Accurate spin densities can be calculated when the three components of the ^{13}C hyperfine tensors (including signs) are known. Since we know only $|A_{zz}|$ for the 1- and 4-carbonyl carbons and can only determine an upper limit for $|A_{xx}|$ and $|A_{yy}|$, we are not yet able to definitively calculate the corresponding spin densities. From model systems studies, it has been shown that the sign of the isotropic hyperfine coupling (a_{iso}) in a protic environment is positive; thus, the large A_{ZZ} component must be positive, and since the trace of the dipolar part of the **hf** tensor must be zero, A_{XX} and A_{YY} must be both negative (*21*, *24*, *40*, *41*).

However, the present data allow us to draw a few tentative conclusions. The asymmetry ($||^{13}C_1-A_{zz}| - |^{13}C_4-A_{zz}||$) of

Table 1: ^{13}C-hf Tensor Principal Values (in mT) of $Q_H^{\bullet-}$ in *bo*$_3$ Containing UQ-2 Specifically Labeled at the 1- and 4-Carbonyl Positions[a]

	^{13}C-UQ-2$^{\bullet-}$	^{13}C-UQ-3$^{\bullet-}$				^{13}C-UQ-10$^{\bullet-}$	
	$Q_H^{\bullet-}$ [b]	isopropanol[c]	DME/mTHF[d]	$Q_B^{\bullet-}$ [c]	$Q_A^{\bullet-}$ [c]	$UQ_{10}^{\bullet-}$(isoprop)[e]	$Q_A^{\bullet-}$ [e]
$^{13}C_1$-A_{XX}	−0.15 (5)[f]	−0.43 (6)	−0.43 (8)	−0.39 (6)	−0.45 (6)	n.d.[g]	0.55 (5)
$^{13}C_1$-A_{YY}	−0.45 (5)	−0.37 (6)	−0.54 (8)	−0.47 (6)	−0.52 (6)	n.d.	0.65(5)
$^{13}C_1$-A_{ZZ}	+1.10 (3)	+1.09 (2)	+0.73 (2)	+0.99 (2)	+0.81 (2)	1.13 (3)	0.80 (3)
$^{13}C_4$-A_{XX}	−0.25 (5)	−0.40 (6)	−0.47 (8)	−0.36 (6)	−0.33 (6)	n.d.	<0.25 (5)
$^{13}C_4$-A_{YY}	−0.37 (5)	−0.35 (6)	−0.55 (8)	−0.37 (6)	−0.35 (6)	n.d.	<0.25 (5)
$^{13}C_4$-A_{ZZ}	+0.72 (3)	+1.15 (2)	+0.73 (2)	+1.15 (2)	+1.25 (2)	1.10 (3)	1.27 (3)
$\lvert^{13}C_1$-A_{zz}- $^{13}C_4$-$A_{zz}\rvert$	0.38	0.06	0.00	0.16	0.44	0.03	0.47

[a] Comparison with $Q_A^{\bullet-}$ and $Q_B^{\bullet-}$ in bRC and with ubiquinone anion radicals in organic solvents. [b] This paper. [c] Ref *21*. [d] Ref *24*. [e] Ref *20*. [f] Numbers in parentheses are the errors in the last digit. [g] n.d.: not determined.

about 4 G contrasts with that of UQ-3$^{\bullet-}$ measured in 2-propanol, where very similar values are observed at both positions (see Table 1) (*21*, *24*). Although the $^{13}C_1$ A_{zz} **hf** component lies in the range of those previously determined for ^{13}C-ubiquinone anions in 2-propanol, ^{13}C-UQ-3$^{\bullet-}$ in Q_A and Q_B and ^{13}C-UQ-10$^{\bullet-}$ in Q_A (refs *20* and *21*, see Table 1), the $^{13}C_4-A_{zz}$ **hf** component reveals a remarkably small value of about 7 G, which is quite similar to the values determined for UQ-0$^{\bullet-}$ and UQ-3$^{\bullet-}$ in DME/mTHF where no hydrogen bonds are formed (*24*).

Previous studies on quinones in vitro have demonstrated that the solvent surrounding has a strong effect on the ^{13}C **hf** couplings at positions 1 and 4. This effect is caused by the presence or absence of hydrogen bonding to the two carbonyl positions that directly influences the distribution of electron spin density over the ring, leading to a change of the polarization of the 2p orbital of the carbon responsible for the ^{13}C hyperfine coupling (*25*−*27*). The shift of spin density in semiquinone anion radicals can be understood from a simple valence model (*42*), recently confirmed by theoretical calculations on durosemiquinones and asymmetrically hydrogen-bonded phyllosemiquinones (*36*, *37*). The formation of a hydrogen bond to one of the carbonyl oxygens of the semiquinone leads to a shift of spin density and charges within the semiquinone ring. The bound oxygen will possess a larger negative charge to stabilize the hydrogen bonding interaction; thus, the spin density will be partly shifted within the semiquinone. When a strong hydrogen bond to O_1 (respectively, O_4) is formed, increase in spin density at carbon C_1, C_3, C_5, and O_4 (respectively, C_2, C_4, C_6, and O_1) is expected. This effect also correlates directly with the magnitude of the $^{13}C-A_{ZZ}$ components.

Thus the measurements performed here give direct and clear evidence that the $^{13}C_4$ **hf** tensor is more isotropic than the $^{13}C_1$ tensor (i.e., that the electron spin density on the C_4 is lower than that on the C_1 indicating that the stronger hydrogen bond is formed to O_1). This is in agreement with measurements of the proton methyl hyperfine couplings at position 5 (*13*−*15*), which are an indirect probe of the unpaired electron density.

In contrast with the situation in a frozen solution of 2-propanol or DME/mTHF, where the electron spin densities (and consequently the ^{13}C **hf** couplings) are similar for carbons at positions 1 and 4, the corresponding A_{ZZ} **hf** couplings determined here differ considerably and especially the very small value observed for C_4 is consistent with a strongly asymmetric or one-sided binding of $Q_H^{\bullet-}$ in its binding pocket. The magnitude of this asymmetry is of similar magnitude to that observed for $Q_A^{\bullet-}$ and much stronger than that of $Q_B^{\bullet-}$ (see Table 1). Their differences were presented as being consistent with Q_B functioning more like a quinone in protic solution (i.e., acting as a $2e^-/2H^+$ acceptor (*3*, *21*, *24*)). Following this reasoning, this suggests that Q_H acts more like Q_A with regard to its function as an intermediate electron donor in the protein.

Moreover, although the $^{13}C_1$ A_{zz} **hf** coupling of $Q_H^{\bullet-}$ lies in the range of couplings determined previously for the above-mentioned ubisemiquinones, the value for $^{13}C_4$ A_{zz} has an unusually small value, very close to the smallest value determined so far on ubiquinones in aprotic solvents, which suggests that this carbonyl oxygen is not hydrogen bonded.

This appears rather unusual and is interpreted as strongly one-sided hydrogen bonding of $Q_H^{\bullet-}$ to the protein. There is currently only one other example in the literature where such an effect could be expected, although no direct measurements have been performed to date, the secondary electron acceptor A_1 in photosystem I (PS I) as revealed in the recently refined 2.5 Å X-ray structure of PS I from *Synechococcus elongatus* (*43*). Recent density functional calculations (*44*) performed on $A_1^{\bullet-}$ concluded that one-sided hydrogen bonding could explain some of the unusual ^{1}H-hfc values that have been observed for A_1 (*45*), which are also similar to those observed here. This would further support the proposal of a one-sided bonding model for $Q_H^{\bullet-}$.

ENDOR studies performed on $Q_H^{\bullet-}$ have previously shown the presence of exchangeable protons in the immediate environment, which were assigned to hydrogen-bonded protons to the quinone (*14*, *15*).

Two **hf** couplings have been assigned to the same axial hyperfine tensor and by comparison with ubisemiquinones in 2-propanol where two different tensors have been resolved (*34*, *46*), it was concluded that stronger hydrogen bonds to the carbonyl oxygens than are present in 2-propanol are formed to the semiquinone in its binding site (*15*).

Further, after comparison with ENDOR data from plastoquinone-substituted samples, Hastings et al. (*15*) postulated a symmetrical hydrogen-bonding environment in contrast to our findings using ubiquinone derivatives. The model presented here does not, however, exclude multiple hydrogen bonding to the 1-carbonyl oxygen as proposed in the modeled Q_H binding site. It is important to note that the observed $^{13}C_4$ **hf** tensor is difficult to reconcile with strong hydrogen bonding to the 4-carbonyl oxygen.

A recent study of the binding of UQ-2 in the cytochrome *bo*$_3$ by FTIR spectroscopy using the same labeled quinones as presented in this work suggested mainly symmetrical and rather weak hydrogen bonding to the oxidized and fully reduced states, although the anion radical state was not

investigated (*28*). Possible reasons for this difference could be a different binding of $Q_H^{\bullet-}$and Q_H and/or a pH-dependent binding of $Q_H^{\bullet-}$.

The first case has been suggested for Q_A (*47*) and shown for Q_B (*48*) in bRC, and the second case has been clearly demonstrated for $Q_A^{\bullet-}$ in photosystem II using HYSCORE spectroscopy (*49*). Such a stabilization of the semiquinone state could be a factor for optimum electron transfer and could depend on the pH, as it has been shown for the intramolecular electron transfer from ubisemiquinone to heme *b* by using the pulse radiolysis technique (*50*).

In the recent ESEEM study of the native $Q_H^{\bullet-}$ radical anion, a strong interaction of the unpaired electron spin with a nitrogen nucleus was observed (*13*). The current study supports the idea that this coupling, suggested to occur via a hydrogen bond, is to the side of the quinone corresponding to the 1-carbonyl position. On the basis of the knowledge of the quadrupolar parameters (K, η) and their comparison with those obtained for other membrane−protein bound semiquinone radicals and model systems, it was assigned to a peptide nitrogen, although an arginine residue cannot be excluded. Such an arginine has been proposed as hydrogen-bond donor to the quinone. If this were the case, the proposed quinone orientation would be supported by this work (i.e., the 1-carbonyl oxygen would form a strong hydrogen bond to Arg71). From both EPR and FTIR measurements on mutant cytochrome bo_3 (Asp75) from *E. coli*, it has been proposed that this amino acid could interact with the semiquinone (*51*, *52*). ESEEM measurements on mutants of the above-cited amino acids could be useful to study this hypothesis and are currently being performed in our laboratory.

CONCLUSIONS

Using a multifrequency EPR approach, clear evidence is obtained for the asymmetric electronic structure of the $Q_H^{\bullet-}$ radical in the bo_3 QOX from *E. coli*. By comparison with data on ubiquinones measured in vitro, it is suggested to form strongly asymmetric or one-sided hydrogen bonding to the protein. In contrast to the binding of Q_A in bRCs, the strong hydrogen bond formed here is to the 1-carbonyl position (which points directly to heme *b*) and not to the 4-carbonyl position. In bRCs, Q_A links a one-electron process to a two-electron process, whereas here Q_H links a two-electron process to a one-electron process and is thus a possible explanation of the observed difference. This may also be an indication of the direction of electron-transfer to heme *b* and thus of the orientation of Q_H in the protein that now has to be examined in detail.

ACKNOWLEDGMENT

We would like to thank Dr. Petra Hellwig (University of Frankfurt, Germany) for providing unpublished data and useful discussions, Prof. Klaus-Peter Dinse (TU Darmstadt, Germany) for the use of the W-band EPR spectrometer, and the EPR division of Bruker Biospin (Rheinstetten, Germany) for the possibility of performing the Q-band EPR measurements.

REFERENCES

1. Trumpower, B. L. (1982) *Function of Quinones in Energy Conserving Systems*, Academic Press, New York.
2. Shinkarev, M. Y., and Wraight, C. A. (1993) in *The Photosynthetic Reaction Center* (Deisenhofer, J., and Norris, J. R. Eds.) Vol. 1, pp 194−255, Academic Press, San Diego.
3. Lubitz, W., and Feher, G. (1999) *Appl. Magn. Reson. 17*, 1−48.
4. Breton, J., Burie, J. R., Berthomieu, C., Berger, G., and Nabedryk, E. (1994) *Biochemistry 33*, 4953−4965.
5. Zhao, X., Ogura, T., Okamura, M., and Kitagawa, T. (1997) *J. Am. Chem. Soc. 119*, 5263−5264.
6. Van Liemt, W. B. S., Boender, G. J., Gast, P., Hoff, A. J., Lugtenburg, J., and de Groot, H. J. M. (1995) *Biochemistry 34*, 10229−10236.
7. Mogi, T., Tsubaki, M., Hori, H., Miyoshi, H., Nakamura, H., and Anraku, Y. (1998) *J. Biochem. Mol. Biol. Biophys. 2*, 79−110.
8. Sato-Watanabe, M., Mogi, T., Miyoshi, H., Iwamura, H., Matsushita, K., Adachi, O., and Anraku, Y. (1994) *J. Biol. Chem. 269*, 28899−29907.
9. Sato-Watanabe, M., Mogi, T., Ogura, T., Kitagawa, T., Miyoshi, H., Iwamura, H., and Anraku, Y. (1994) *J. Biol. Chem. 269*, 28908−28912.
10. Abramson, J., Riistama, S., Larsson, G., Jasaitis, A., Svensson-Ek, M., Laakkonen, L., Puustinen, A., Iwata, S., and Wikström, M. (2000) *Nature Struct. Biol. 7*, 910−917.
11. Sato-Watanabe, M., Itoh, S., Mogi, T., Matsuura, K., Miyoshi, H., and Anraku, Y. (1995) *FEBS Lett. 374*, 265−269.
12. Ingledew, W. J., Ohnishi, T., and Salerno, J. C. (1995) *Eur. J. Biochem. 227*, 903−908.
13. Grimaldi, S., MacMillan, F., Ostermann, T., Ludwig, B., Michel, H., and Prisner, T. (2001) *Biochemistry 40*, 1037−1043.
14. Veselov, A. V., Osborne, J. P., Gennis, R. B., and Scholes, C. P. (2000) *Biochemistry 39*, 3169−3175.
15. Hastings, S. F., Heathcote, P., Ingledew, W. J., and Rigby, S. E. J. (2000) *Eur. J. Biochem. 267*, 5638−5645.
16. Michel-Beyerle, M. E., Ed. (1996) in *The Reaction Center of Photosynthetic Bacteria: Structure and Dynamics*, Springer-Verlag, Berlin, Germany.
17. Breton, J., Burie, J. R., Boullais, C., Berger, G., and Nabredyk, E. (1994) *Biochemistry 33*, 12405−12415.
18. Brudler, R., de Groot, H. J. M., van Liemt, W. B. S., Steggerda, W. F., Esmeijer, R., Gast, P., Hoff, A. J., Lugtenburg, J., and Gerwert, K. (1994) *EMBO J. 13*, 5523−5530.
19. Breton, J., Boullais, C., Burie, J. R., Nabredyk, E., and Mioskowski, C. (1994) *Biochemistry 33*, 14378−14386.
20. Van den Brink, J. S., Spoyalov, A. P., Gast, P., van Liemt, W. B. S., Raap, J., Lugtenburg, J., and Hoff, A. J. (1994) *FEBS Lett. 353*, 273−276.
21. Isaacson, R. A., Abresch, E. C., Lendzian, F., Boullais, C., Paddock, M. L., Mioskowski, C., Lubitz, W., and Feher, G. (1996) in *The reaction center of photosynthetic bacteria, structure and dynamics* (Michel-Beyerle, M.-E., Ed.) pp 353−367, Springer-Verlag, Berlin, Germany.
22. Brudler, R., de Groot, H. J., van Liemt, W. B., Gast, P., Hoff, A. J., Lugtenburg, J., and Gerwert, K. (1995) *FEBS Lett. 370*, 88−92.
23. Breton, J., Boullais, C., Berger, G., Mioskowski, C., and Nabredyk, E. (1995) *Biochemistry 34*, 11606−11616.
24. Nimz, O., Lendzian, F., Boullais, C., and Lubitz, W. (1998) *Appl. Magn. Reson. 14*, 255−263.
25. Karplus, M. A., and Fraenkel, G. K. (1961) *J. Chem. Phys. 35*, 1312−1323.
26. Das, M. R., and Fraenkel, G. K. (1965) *J. Chem. Phys. 42*, 1350−1360.
27. O'Malley, P. J. (1998) *Chem. Phys. Lett. 291*, 367−374.
28. Hellwig, P., Mogi, T., Tomson, F. L., Gennis, R. B., Iwata, J., Miyoshi, H., and Mäntele, W. (1999) *Biochemistry 38*, 14683−14689.
29. Rumbley, J. N., Furlong Nickels, E. F., and Gennis, R. B. (1997) *Biochim. Biophys. Acta 1340*, 131−142.
30. Schröter, T., Winterstein, C., Ludwig, B., and Richter, O.-M. H. (1998) *FEBS Lett. 432*, 109−112.
31. Faller, P., Maly, T., Rutherford, A. W., and MacMillan, F. (2001) *Biochemistry 40*, 320−326.
32. Prisner, T. F., Lyubenova, S., Atabay, Y., MacMillan, F., Kröger, A., and Klimmek, O. (2003) *J. Biol. Inorg. Chem. 8*, 419−426.
33. Burghaus, O., Plato, M., Rohrer, M., Möbius, K., MacMillan, F., and Lubitz, W. (1993) *J. Phys. Chem. 29*, 7639−7647.
34. MacMillan, F., Lendzian, F., and Lubitz, W., (1995) *Magn. Reson. Chem. 33*, 81−93.
35. Knüpling, M., Törring, J. T., and Un, S. (1997) *Chem. Phys. 219*, 291−304.

36. O'Malley, P. J. (1998) *J. Phys. Chem. A 102*, 248−253.
37. O'Malley, P. J. (1999) *Biochim. Biophys. Acta 1411*, 101−113.
38. Boiden Pedersen, J., Hansen C. E. M., Parbo, H., and Muus, L. T. (1975) *J. Chem. Phys. 63*, 2398−2405.
39. Isaacson, R. A., Lendzian, F., Abresch, E., Lubitz, W., and Feher, G. (1995) *Biophys. J. 69*, 311−322.
40. Strauss, H. L., and Fraenkel, G. K. (1961) *J. Chem. Phys. 35*, 1738.
41. Samoilova, R. I., Van Liemt, W. B. S., Steggerda, W. F., Lugtenburg, J., and Hoff, A. J. J. (1994) *J. Chem. Soc., Perkin Trans. 2*, 609−614.
42. MacMillan, F., Lendzian, F., Renger, G., and Lubitz, W. (1995) *Biochemistry* 8144−8156.
43. Jordan, P., Fromme, P., Witt, H. T., Klukas, O., Saenger, W., and Krauss, N. (2001) *Nature 411*, 909−917.
44. Kaupp, M. (2002) *Biochemistry 41*, 2895−2900.
45. Rigby, S. E. J., Heathcote, P., and Evans, M. C. W. (1996) *Biochemistry 35*, 6651−6656.
46. Rohrer, M., MacMillan, F., Prisner, T. F., Gardiner, A., Möbius, K., and Lubitz, W. (1998) *J. Phys. Chem. B 102*, 4648−4657.
47. Kropacheva, T. N., van Liemt, W. B. S., Raap, J., Lugtenburg, J., and Hoff, A. J. (1996) *J. Phys. Chem. 100*, 10433−10442.
48. Stowell, M. H., McPhilips, T. M., Rees, D. C., Soltis, S. M., Abresch, E., and Feher, G. (1997) *Science 276*, 812−816.
49. Deligiannakis, Y., Hanley, J., and Rutherford, A. W. (1999) *J. Am. Chem. Soc. 121*, 7653−7664.
50. Kobayashi, K., Tagawa, S., and Mogi, T. (2000) *Biochemistry 39*, 15620−15625.
51. Hellwig, P., Barquera, B., and Gennis, R. B. (2000) *Biochemistry 40*, 1077−1082.
52. Hellwig, P., Yano, T., Ohnishi, T., and Gennis, R. B. (2002) *Biochemistry 41*, 10675−10679.

BI034010Z